SAND2005-7698C

Effect of EGR on Diesel Premixed-Burn Equivalence Ratio

Cherian A. Idicheria and Lyle M. Pickett*
Sandia National Laboratories, P. O. Box 969, MS 9053, Livermore, CA 94551, USA

Submitted to 31st International Symposium on Combustion

Colloquim: IC Engines and Gas Turbine Combustion

Key words: Diesel combustion, EGR, n-heptane

Word Count:

Main Text (excluding abstract)	Word processor count utility	3805
Equation	(2+2)x7.6x1	30
Figures and captions		
Fig. 1	(38+10)x2.2x1 + 25	131
Fig. 2	(51+10)x2.2x1 + 8	142
Fig. 3	(89+10)x2.2x1 + 26	244
Fig. 4	(55+10)x2.2x1 + 26	169
Fig. 5	(102+10)x2.2x2 + 22	515
Fig. 6	(51+10)x2.2x1 + 17	151
References	(16+2)x2.3x7.6	314
Tables		
Table 1	(11+2)x7.6	99
Table 2	(6+2)x7.6	61
Table 3	(6+2)x7.6	61
Total		5722

* Corresponding Author: Fax: +1 925 294 1004, E-mail: LMpicke@sandia.gov

Abstract

The effect of exhaust-gas recirculation (EGR) on the equivalence ratio of the premixed-burn mixture in diesel combustion was investigated experimentally. The ambient oxygen concentration was systematically decreased from 21% to 10% in a constant-volume combustion vessel to simulate EGR effects in engines. Pressure measurements and time-resolved imaging of high-temperature chemiluminescence were used to characterize the temporal and spatial ignition and premixed burn characteristics of n-heptane diesel jets. With increasing EGR, ignition delay increases and the location of ignition and pemixed burn occurs further downstream from the nozzle. Subsequent to first ignition, high temperature reactions stabilize at a quasi-steady lift-off length, showing that lift-off is a bounding parameter for determining premixed-burn region. The equivalence ratio of the fuel-ambient mixture in the premixed-burn region was measured using planar laser Rayleigh scattering. Distribution functions of fuel-oxygen mass show more mass is mixed into the premixed-burn region with increasing EGR, but the equivalence ratio of this mixture increases slightly. The study shows that an increasing ignition delay with increasing EGR does not necessarily decrease the equivalence ratio as would be desired for reducing soot formation in low-temperature combustion engines. However, measures to improve fuel-air mixing, such as shortened injection durations coupled to long ignition delay, could decrease equivalence ratio.

Introduction

Concepts for low-temperature diesel combustion generally utilize high levels of cooled exhaust-gas recirculation (EGR). EGR reduces flame temperature, thereby reducing nitrogen oxide (NOx) emissions, but EGR also typically increases particulate matter (PM) emissions [1]. However, researchers have shown that EGR can significantly reduce PM emissions in some combustion strategies [2-5].

The PM emissions reduction appears related to an increase in ignition delay, caused by cooled EGR, which provides more time for mixing before combustion and the potential for a decrease in the equivalence ratio (ϕ) of the igniting fuel-ambient mixture. The PM reduction is most significant when the ignition delay exceeds the injection duration and there is a high degree of fuel-ambient mixing. The ensuing combustion appears highly premixed and researchers conclude that local ϕ are sufficiently reduced so as to prevent soot formation ($\phi < 2$), while EGR and fuel-lean mixtures reduce flame temperatures and suppress NOx formation [3,5].

The above combustion systems appear promising, but are currently restricted to low-load conditions, partially because of the requirement that injection end prior to ignition. In practice, high-load conditions are achieved through injection durations that exceed the ignition delay. In addition, use of EGR lowers charge-gas oxygen concentration, which can ultimately limit the maximum achievable load.

A reduced oxygen concentration can also hinder attainment of low ϕ in the igniting fuel-ambient mixture. This is because the ambient-to-fuel stoichiometric ratio $(A/F)_{st}$ increases with increasing EGR, implying that more ambient mass must be mixed with fuel to achieve the same ϕ. If mixing parameters are left constant, the time required

to mix to a given ϕ will be longer. A decrease in ϕ with increasing EGR is possible only if the increase in ignition delay can compensate for this longer-mixing-time requirement. Shortening the injection duration to be less than the ignition delay will tend to reduce ϕ, irrespective of EGR condition. Therefore, for the engine studies above it is unknown if the longer ignition delay is primarily responsible for the reduction in soot formation and ϕ or if additional measures that increase mixing, like shortened injection duration, are needed to reduce ϕ.

To assess this question, in this study we identify and perform direct measurement of ϕ in the premixed-burn region of a fuel spray. The ambient oxygen concentration is varied while other engine-like conditions are held constant. Moreover, the injection duration exceeds the ignition delay to keep mixing parameters constant up until the time of premixed burn and to focus on conditions needed to extend low-emission, low-temperature combustion to higher engine load.

Experimental Details

Experiments were conducted in a constant-volume combustion vessel under simulated, quiescent diesel engine conditions. Previous publications provide detailed description of the combustion vessel [6,7]. The vessel has a cubical combustion chamber (108 mm) with optical access provided by side-port windows. A fuel injector is mounted in a metal side-port such that the diesel spray is directed into the center of the chamber.

The procedure for simulating engine conditions is started by filling the vessel to a specified density with a premixed combustible-gas mixture that is ignited to create a high-temperature, high-pressure environment. The pressure and temperature slowly decrease as combustion products cool over a relatively long time (~1-2 s) until reaching

desired experimental conditions. The fuel injector is then triggered, and ignition and combustion processes ensue. The ambient gas composition at injection is varied by adjusting the initial premixed combustible-gas mixture. In this study, four different ambient oxygen concentrations (21% - 10%) were considered to simulate the effect of EGR in an engine (Table 1). A vaporizing fuel jet, without combustion, was also simulated by injecting fuel into an ambient that had 0% oxygen. This non-reacting environment was used to perform quantitative ϕ measurements.

A common-rail fuel injector was operated at conditions given in Table 2. The injector was fitted with a single-orifice, mini-sac-type injector tip and used n-heptane fuel [8]. The experimental conditions were chosen because of their similarity to conditions expected near top-dead-center (TDC) in an engine. Multiple injections were performed at the same experimental conditions, to obtain statistical convergence. The time after start of injection (ASI) for measurements was always less than the injection duration.

Various diagnostics were employed in the experiments. Pressure measurements were used to determine the time of the premixed burn relative to the start of injection (ignition delay). Time-resolved imaging of high-temperature, broadband chemiluminescence was used to characterize the ignition and premixed-burn region of the fuel jet. The imaging was accomplished using a high-framing-rate CMOS camera (17.9 KHz) fitted with a 50 mm Nikon f/1.2 lens. Quantitative equivalence ratio measurements in the vaporizing fuel jet were made using planar laser Rayleigh scattering (PLRS). The light source was a Nd:YAG laser (532 nm) with a pulse energy of 150 mJ. The laser beam was formed into a collimated 40 mm wide, 300 μm thick sheet and passed through the fuel jet center. The Rayleigh signal was spectrally filtered using a 10 nm (FWHM)

filter and imaged using a cooled back-illuminated CCD camera with a resolution of 1024x1024 pixels and fitted with a 105 mm Nikon f/1.8 lens.

The PLRS technique implemented in the current study for quantitative ϕ measurement is similar to one developed for a Diesel optical engine [9]. Alternate measurement techniques for ϕ in high-temperature diesel sprays include laser-induced fluorescence and Mie scattering [10-12]. However, these techniques require doping of the fuel with a significant amount of tracer and calibration for substantial fluorescence temperature dependency [10]. Rayleigh scattering, on the other hand, utilizes elastic scattering from molecules but suffers from interference from other elastic-scattering sources such as particles or windows. Rayleigh scattering cross-sections (σ_i) are known for common molecules and are a function of refractive index (n_i) and depolarization ratio (ρ_v) [9,13-15]. The dependency of σ_i on temperature is negligible (<2% at 532 nm) [9]. σ_i, n_i and ρ_v are listed in Table 3 for the ambient gases and fuel used in this study. The ratio of fuel-to-ambient Rayleigh scattering cross-section (σ_f/σ_a) is 55, using a mole-fraction-weighted ambient with 0% oxygen.

Similar to the methodology in [9], an adiabatic mixing model was applied to estimate the temperature in the vaporizing and mixing fuel jet for all fuel-ambient ratios. Following this assumption, and the fact that the probed species is a binary mixture of fuel and ambient, the ratio of the Rayleigh intensity from the jet (I_j) to the ambient (I_a) can be derived as [9]:

$$\frac{I_j}{I_a} = \frac{\left(\sigma_f/\sigma_a\right) + \left(N_a/N_f\right)_{st}/\phi}{1 + \left(N_a/N_f\right)_{st}/\phi} \frac{T_a}{T_{mix}} \qquad (1)$$

where $(N_a/N_f)_{st}$ is the ratio of stoichiometric ambient-fuel number density and T_{mix} is adiabatic mixture temperature. For a given intensity ratio, there is a unique combination of ϕ and T_{mix} that satisfies Eq (1) for a particular ambient oxygen condition.

The Rayleigh technique employed for ϕ measurements is illustrated in Fig. 1, which is a composite image of the vaporizing n-heptane fuel jet visualized using two different techniques. The left image (till 16 mm) shows Mie scattering from the liquid-phase of the vaporizing fuel jet. The right image is Rayleigh scattering from the ambient and the vapor-phase of the fuel jet. Scattering from liquid fuel extends only to 8 mm, which distance is determined by fuel type, boiling point temperature (95°C at 1 atm for n-heptane), nozzle size, and mixing with high-temperature ambient [7]. Positioning of the PLRS laser sheet and camera field-of-view downstream of the liquid penetration ensured no interference from liquid droplets.

The Rayleigh image (Fig. 1) highlights some of the advantages and difficulties of PLRS technique. A major advantage is that scattering from the ambient (I_a) is measured, providing an in-situ calibration for spatial variation in laser sheet intensity. Spatial variations of intensity are typical from shot-to-shot in most laser sheets and are evident in Fig. 1. The upper part of the Rayleigh image also shows significant beam steering as the laser sheet passes through the jet. As the laser sheet is nearly collimated, the I_a at an axial position is used to compute the ratio (I_j/ I_a) in Eq (1). To remove effects of beam steering, or other variation in laser intensity perpendicular to the jet axis, a linear interpolation between I_a values immediately outside the top and bottom of the jet was implemented in regions of the jet.

Other image corrections included subtraction of camera dark charge and thermal emission (thermal signature when there is no laser pulse) and, most significant, subtraction of background flare from window reflections. In the current study, a two step process was followed to correct for this background interference. As a first step, a mean background image of laser scatter from an evacuated vessel was subtracted. However, this step did not ensure complete removal of background flare as some flare remained outside of the laser sheet in vaporizing-jet images, leaving uncertainty in the I_a and I_j values. To ascertain the correct value of I_a, multiple experiments were performed at high-pressure and temperature conditions without fuel injection using a thin laser sheet (5 mm by adjustable beam blocks) to minimize sources of background flare and enable accurate I_a measurement. In this manner, a calibration image for mean values of I_a along the jet axis was generated. The final step for flare correction of individual images was to apply a scale factor to the mean background image before correction such that the mean I_a after background subtraction is in agreement with the mean I_a in the calibration image.

The sources of error when using Rayleigh scattering technique are discussed at length in [9]. As alluded to above, the largest source of error is the inability to completely remove the background scatter that can bias the estimate of I_a. To minimize background flare, vessel walls were coated with a high-temperature, absorptive black paint and windows were cleaned often to remove scatter from deposits. Other smaller sources of error include laser sheet non-uniformity, beam steering effects and Mie scattering interference from the particles in the jet (not fuel droplets), which is evident in several regions of the PLRS image in Fig. 1. These particles could not be removed completely by filtering of the fuel and the problem was more extreme for early time after the start of

injection (ASI) for an unexplained reason. Consequently, particles were removed in post-processing from instantaneous images using a 12x12 median filter, unlike the raw image of Fig. 1. The effect of using the median filter to remove the particles was investigated. Though the absolute ϕ is affected, the trend across the different ambient oxygen conditions is preserved.

Results and Discussion

This section is organized as follows: First, pressure measurements are used to describe the effect of EGR on ignition delay. Second, the spatial evolution of ignition and premixed burn is shown using time-resolved imaging data. Third, Rayleigh measurements are presented to quantify the mixture ϕ at the premixed-burn region for different EGR conditions.

Figure 2 shows the pressure rise (above) and apparent heat-release rate (AHRR) (below) plotted as a function of time ASI, for the different EGR conditions. The data shown is averaged over many (~150-200) injections. To capture the pressure rise due to heat-release effects alone, the pressure data has been corrected for the pressure decrease due to vessel cooling and fuel vaporization effects (done by measuring mean pressure drop when injecting fuel into an ambient with no oxygen). From the pressure-rise plot, the increase in ignition delay with increasing EGR is evident. For example, the ignition delay for the 10% oxygen is approximately 1.0 ms when compared to 0.4 ms for the 21% oxygen (Table 1).

The AHRR plot shows small heat release caused by a cool flame [16], followed by rapid high-temperature ignition and premixed burn. The ignition delay time τ_{id} is defined as the beginning of this high-temperature pressure rise and it corresponds to

approximately half the peak AHRR. Figure 2 shows that the peak AHRR during the premixed burn decreases with increasing EGR. Possible reasons for the decline include slower chemical kinetics because of dilution or lack of oxygen entrainment because of reduced ambient oxygen. However, the time available for premixing is longer because of the increased τ_{id} for high-EGR conditions. The duration of the premixed burn also increases with increasing EGR. Therefore, even though the peak AHRR decreases, the igniting mixture may release more total energy during the premixed burn. Examination of the cumulative pressure rise at the end of the premixed burn (vertical lines in Fig. 2) shows that the pressure rise at this time increases with increasing EGR, indicating higher heat release. However, this result does not necessarily prove that there was more oxygen entrainment at the beginning of the premixed burn because the lengthened premixed burn allows additional time for mixing.

The pressure rise and AHRR measurements show the temporal effect of EGR on mixture ignition. In Fig. 3, images of high-temperature, broadband chemiluminescence from a single injection event are presented to elucidate both the temporal and spatial location of ignition and premixed burn. Two image sets are shown; 15% and 10% oxygen, with images for increasing time ASI stacked one below the other. The quasi-steady lift-off length (measured using OH chemiluminescence [8]) for the particular oxygen condition is shown as a dashed white line. For the image sequences shown, evidence of first ignition for the 15% oxygen and 10% oxygen occur at 615 μs and 1062 μs, respectively; consistent with τ_{id} estimates from pressure measurements. With increasing EGR, the location of first ignition occurs further downstream and the quasi-steady lift-off length increases [8].

For each oxygen condition, combustion develops rapidly from the first ignition sites, expanding to outline the head of the penetrating jet and eventually stabilizing near the quasi-steady lift-off length (towards the injector). Values for the instantaneous lift-off length were obtained by identifying the high-temperature chemiluminescence region closest to the injector for each frame in the time-resolved sequences. The mean lift-off length from ten injections is shown in Fig. 4 as a function of time ASI for each oxygen condition. For individual injections where ignition has not occurred at a particular time ASI, due to injection-to-injection variations, an estimate of the jet penetration distance at that time ASI [6] is used as the lift-off length.

Consistent with Fig. 3, the lift-off length decreases during ignition and premixed burn and quickly relaxes to a quasi-steady value [16]. Quasi-steady lift-off lengths obtained from OH chemiluminescence imaging, rather than broadband chemiluminescence, are shown in Fig. 4 (dashed lines) [8]. The two measurements are in close agreement, but the broadband chemiluminescence results indicate a slightly longer lift-off length than the OH chemiluminescence results. Reasons for this difference include: first, the OH chemiluminescence measurements are obtained over a larger dataset (>100 compared to 10). Second, broadband chemiluminescence can be affected by interference from soot luminosity, which exists during quasi-steady combustion (see saturated regions in 15% oxygen in Fig. 3). In contrast, the OH chemiluminescence technique is less sensitive to soot luminosity due to spectral filtering. For these reasons, in this paper we rely on the OH chemiluminescence values for lift-off length.

The time-resolved imaging shows that the quasi-steady lift-off length represents an axial position that forms a lower boundary on the region where fuel-ambient mixtures

react during ignition and the premixed burn, while the upper boundary is the head of the penetrating jet. Therefore, for a particular ambient oxygen concentration, the boundary defined above at the time of ignition (τ_{id}) is of interest for evaluation of the ϕ of premixed-burn mixtures. Rayleigh scattering measurements were performed in an inert environment (0% oxygen) corresponding to the τ_{id} for each ambient oxygen concentration. Images were then processed using the $(N_a/N_f)_{st}$ ratio for the particular ambient oxygen concentration (Table 1) and Eq (1) to obtain ϕ values.

Rayleigh scattering measurements were performed in an inert environment for several reasons. First, Rayleigh scattering cross-sections are not preserved if fuel combusts or undergoes significant high-temperature pyrolysis. With oxygen present in the ambient, fuel breakdown begins prior to high-temperature ignition with the formation of a cool flame. However, Senkin simulations at 1000 K and 0% oxygen show that n-heptane decreases by less than 1% in 1 ms, indicating negligible pyrolysis. Second, there is no interference from combustion luminosity, allowing use of a high-quantum-efficiency, slow-gate camera. Note that use of an inert environment to quantify the mixture ϕ of the premixed burn neglects heat-release effects of the cool flame prior to main ignition. However, the cool flame occurs predominately downstream of the lift-off length [16], and has only a mild temperature rise. Accordingly, the cool flame is not expected to significantly alter the spatial location of fuel-ambient mixture preparation upstream of the lift-off length, comparing inert to reacting conditions.

Figure 5 shows the mean (left) and instantaneous (right) images of ϕ for different EGR conditions. The mean ϕ images (contours superimposed) were obtained by

averaging multiple instantaneous images (~20-40). The time ASI of image acquisition is the τ_{id} for a particular EGR condition. The lift-off length is shown as a dashed white line.

Comparing ϕ distributions for different EGR conditions, there are richer mixtures at the same axial location for lower ambient oxygen concentration. This is expected because of the reduced entrainment of oxygen into the jet in a high-EGR environment. However, since the ignition and premixed-burn region (distances greater than the lift-off length) shifts downstream as EGR is varied, the peak ϕ of the mixtures doesn't necessarily change (mean centerline values of 2 to 3). There are also noticeable differences between the structure of the instantaneous and mean ϕ distribution. The transient head and the large-scale turbulent structure of the jet are more prominent in the instantaneous images than in the mean images. As expected, stoichiometric values are along the jet periphery and ϕ decreases with increasing distance along the jet centerline.

To better compare the fuel-ambient distributions in the premixed-burn region, a histogram for the amount of fuel at a given ϕ was computed for the region extending from the lift-off length to the head of the jet. The two-dimensional information was first converted to a jet volume by assuming axi-symmetry and rotating the top and bottom half of the jet through 180° about the centerline (meaning that pixels are weighted by πr). The fuel mass at a given ϕ was then computed using the ideal gas law for each pixel volume. The fuel distribution histogram was generated in a cumulative fashion for each oxygen condition from the set of instantaneous ϕ images with a bin size of $\Delta\phi$=0.1 and is shown in Fig. 6.

Showing the fuel mass distribution with respect to ϕ is preferred for several reasons. As the purpose of this study was to vary EGR, mixtures with the same ϕ and

occupying the same volume will have different fuel mass because of differences in $(N_a/N_f)_{st}$. However, since $\phi \equiv (N_a/N_f)_{st}/(N_a/N_f) = (O/F)_{st}/(O/F)$, where $(O/F)_{st}$ depends only upon the fuel (inert gases in the ambient need not be considered for the latter definition), it is clear that mixtures with the same fuel mass (F) and ϕ will have the same mass of oxygen (O), but occupy different volume if EGR is varied. As the energy released during combustion depends on mass of mixed fuel and oxygen, the potential for heat release during the premixed burn depends on fuel mass at a given ϕ. Hence it is more logical to examine how the fuel mass is distributed with respect to ϕ. On the other hand, a volumetric histogram counting only equivalence ratio will give undue importance to low values of ϕ that contain little fuel.

Figure 6 shows that fuel mass distributions for the premixed-burn region exhibit a monotonic behavior of increasing fuel mass over the range of ϕ with increasing EGR. This suggests that the fraction of fuel available for premixed burn increases with increasing EGR and the cumulative heat release during the premixed burn would increase, if all of the fuel reacts completely. A related implication is that the total oxygen entrained into the ignition region increases with increasing EGR. Assuming complete combustion of the fuel distribution at a given ϕ, the total energy release can be computed and is shown in the legend of Fig. 6.

The increasing energy release with increasing EGR is consistent with the increasing pressure rise at the *end* of the premixed burn (Fig. 2), which *may* be explained by a higher mass of premixed fuel. However, this explanation is not conclusive because the premixed burn duration increases with increasing EGR, allowing progressively more time for additional mixing prior to the end of the premixed burn. Nevertheless, our direct

measurements of ϕ (at the time of τ_{id}), coupled to identification of the premixed-burn region, show that mixtures have potential for increased heat release with increasing EGR, even at the *beginning* of the premixed burn (τ_{id}).

Despite an increasing fraction of fuel available for premixed burn with increasing EGR, Fig. 6 shows that the ϕ of this mixture does not decrease, in fact, there is more fuel mass at fuel-rich ϕ. The average mass-weighted ϕ ($\bar{\phi}$) increases monotonically with increasing EGR, as shown in the legend of Fig. 6.

These results show that an increasing ignition delay with increasing EGR does not necessarily decrease ϕ of the premixed-burn mixture as would be desired for reducing soot formation in low-temperature combustion engines. However, the injection duration was much longer than the ignition delay in this study, to ensure mixing parameters were not affected. If injection were concluded prior to ignition, the fuel distribution for the premixed-burn region would likely shift to lower ϕ, but additional knowledge of the premixed-burn region is required. Real engines also present other scenarios that may be important. For example, engines have confined jets with jet-jet and jet-wall interaction and these interactions are more likely for high-EGR, long-ignition-delay conditions. These effects may shorten the lift-off length when compared to the scenario without jet-jet interaction (e.g. no EGR), and increase the ϕ in the premixed-burn mixture. It is also not clear that ending injection prior to ignition will prevent these interactions.

Conclusions

A study was conducted with the aim of quantifying the mixture equivalence ratio at diesel premixed-burn while changing the EGR condition. The ignition delay and spatial evolution of the ignition and premixed burn was investigated using pressure

measurements and time-resolved broadband high-temperature chemiluminescence imaging, respectively. Ignition and premixed burn was found to occur in a volume downstream of the lift-off length irrespective of the EGR condition. Rayleigh scattering measurements were made in a vaporizing fuel jet to quantify the equivalence ratio distribution during premixed burn. Results show the peak equivalence ratio in the premixed-burn region to have a value of 2-3 for all EGR conditions. Fuel-oxygen mass distributions show a larger mass in the premixed-burn region for higher EGR conditions, implying higher potential for heat release during the premixed burn, but the mean equivalence ratio of this mixture increases slightly.

Acknowledgments

Support for this research was provided by the U.S. Department of Energy, Office of FreedomCAR and Vehicle Technologies. Sandia NNSA #DE-AC04-94AL85000.

References

1. N. Ladommatos, S. Abdelhalim, H. Zhao, *Int. J. Engine Research* 1 (1) (2000) 107-126.
2. K. Akihama, Y. Takatori, K. Inagaki, S. Sasaki, A.M. Dean, *SAE Paper* 2001-01-0655.
3. S. Kimura, O. Aoki, Y. Kitahara, E. Aiyoshizawa, *SAE Paper* 2001-01-0200.
4. R.M. Wagner, J.B. Green Jr., T.Q. Dam, K.D. Edwards, J.M. Storey, *SAE Paper* 2003-01-0262.
5. A.E. Klingbeil, H. Juneja, Y. Ra, R.D. Reitz, *SAE Paper* 2003-01-0341.
6. J.D. Naber, D.L. Siebers, *SAE Paper* 960034.
7. D.L. Siebers, *SAE paper* 980809.
8. C.A. Idicheria, L.M. Pickett, *SAE Paper* 2005-01-3834.
9. C. Espey, J.E. Dec, T.A. Litzinger, D.A. Santavicca, *Combust. Flame* 109 (1997) 65-86.
10. T. Kim, J.B. Ghandhi, *SAE Paper*, 2001-01-3495.
11. G. Bruneaux, *SAE Paper*, 2005-01-2100.
12. G. Bruneaux, *Atomization and Sprays* 11 (2001) 533-556.
13. J.A. Sutton, J.F. Driscoll, *Optics Letters* 29 (22) (2004) 2620-2622.
14. J. Fielding, J.H. Frank, S.A. Kaiser, M.D. Smooke, M.B. Long, *Proc. Combust. Inst.* 29 (2002) 2703-2709.
15. W.C. Gardiner Jr., Y. Hikada, T. Tanzawa, *Combust. Flame* 40 (1981) 213-219.
16. L.M. Pickett, D.L. Siebers, C.A. Idicheria, *SAE Paper* 2005-01-3843.

Table 1

Ambient gas composition and properties

Molar % of ambient gases				$(N_a/N_f)_{st}$ [a]	τ_{id} [b]
O_2	N_2	CO_2	H_2O	n-heptane	[ms]
21.0	69.33	6.11	3.56	51	0.42
15.0	75.15	6.22	3.63	73	0.61
12.0	78.07	6.28	3.65	92	0.83
10.0	80.00	6.33	3.67	110	1.06
0.0	89.71	6.52	3.77	-	-

[a] Stoichiometric ambient-to-fuel number ratio
[b] Ignition delay

Table 2

Ambient and fuel injector conditions

Ambient temperature, T_a	1000 K
Ambient density, ρ_a	14.8 kg/m^3
Orifice pressure drop, ΔP	1500 bar
Orifice diameter, d	100 μm

Table 3

Rayleigh cross sections of molecules at STP and λ=532 nm [13-15]

	N_2	CO_2	H_2O	n-heptane
σ_i x 10^{-27} [cm^2]	5.23	12.02	3.66	309.80
(n_i -1) x 10^4	3.002	4.480	2.533	23.290
ρ_v x 100	1.12	3.49	-	-

LIST OF FIGURE CAPTIONS

Figure 1 Composite image of Mie scattering (left) and Rayleigh scattering (right). The experimental conditions are shown in Table 2 and the ambient corresponds to 0% oxygen.

Figure 2 Pressure rise and AHRR for different EGR conditions.

Figure 3 Time resolved image sequences of ignition and premixed burn for two different oxygen condition. Time ASI on upper left. Dashed white line is quasi-steady lift-off length.

Figure 4 Average lift-off length behavior plotted as a function of time ASI for different EGR conditions. Dashed lines are quasi-steady lift-off length from OH chemiluminescence imaging [8].

Figure 5 Mean (left) and instantaneous (right) equivalence ratio images for the different EGR conditions at time of ignition. Dashed line is lift-off length.

Figure 6 Fuel mass distributions in the premixed-burn region for different EGR conditions. The bin size used was $\Delta\phi$=0.1.

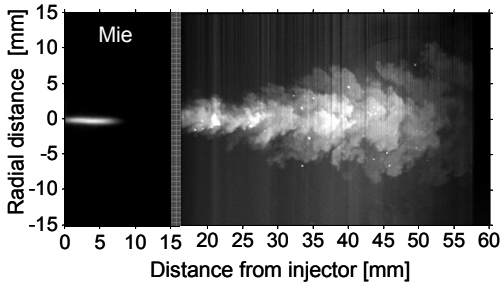

Figure 1. Composite image of Mie scattering (left) and Rayleigh scattering (right). The experimental conditions are shown in Table 2 and the ambient corresponds to 0% oxygen.

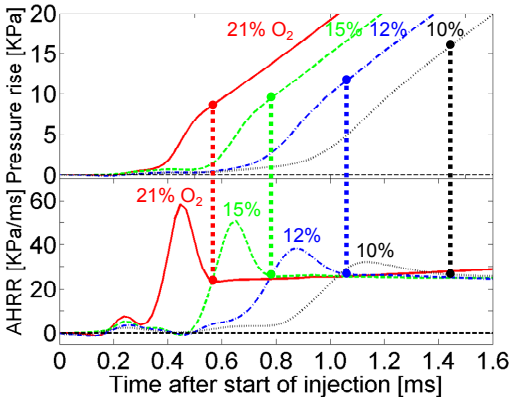

Figure 2. Pressure rise and AHRR for different EGR conditions.

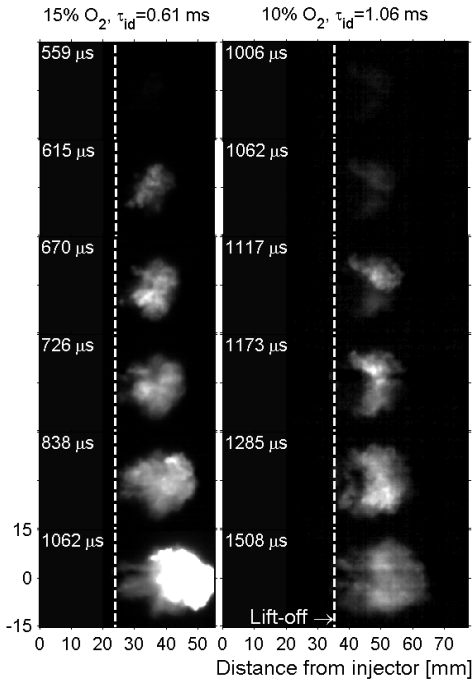

Figure 3. Time resolved image sequences of ignition and premixed burn for two different oxygen condition. Time ASI on upper left. Dashed white line is quasi-steady lift-off length.

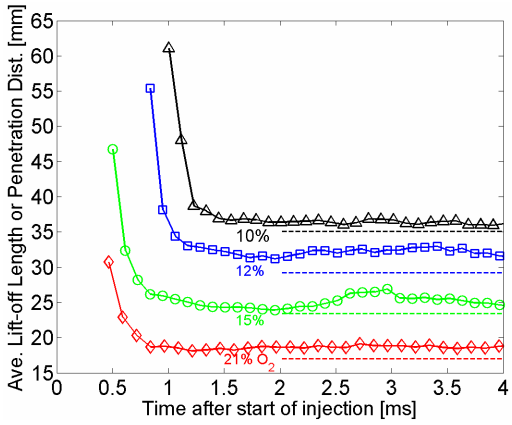

Figure 4. Average lift-off length behavior plotted as a function of time ASI for different EGR conditions. Dashed lines are quasi-steady lift-off length from OH chemiluminescence imaging [8].

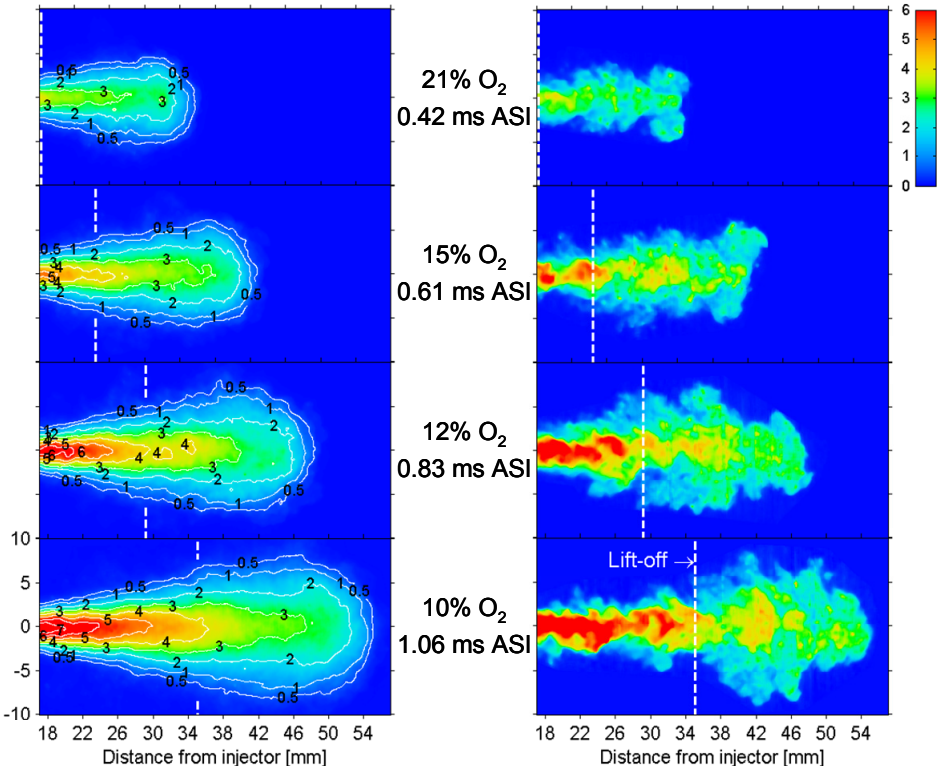

Figure 5. Mean (left) and instantaneous (right) equivalence ratio images for the different EGR conditions at time of ignition. Dashed line is lift-off length.

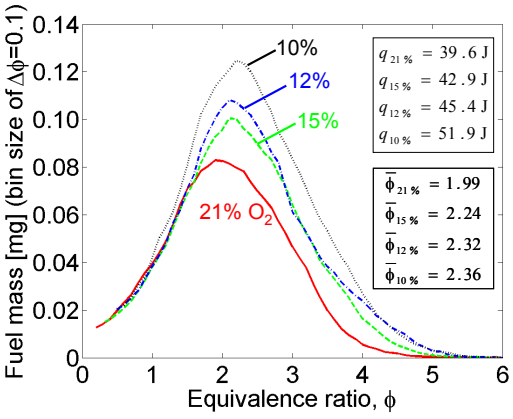

Figure 6. Fuel mass distributions in the premixed-burn region for different EGR conditions. The bin size used was $\Delta\phi$=0.1.